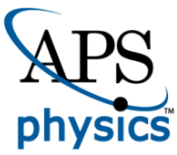

Instabilities of Jammed Packings of Frictionless Spheres Under Load

Ning Xu, Andrea J. Liu, and Sidney R. Nagel

Phys. Rev. Lett. **119**, 215502 — Published 20 November 2017

DOI: 10.1103/PhysRevLett.119.215502

Instabilities of jammed packings of frictionless spheres under load

Ning Xu[1], Andrea J. Liu[2], and Sidney R. Nagel[3]
[1]*CAS Key Laboratory of Soft Matter Chemistry, Hefei National Laboratory for Physical Sciences at the Microscale, and Department of Physics, University of Science and Technology of China, Hefei 230026, P. R. China;*
[2]*Department of Physics and Astronomy, University of Pennsylvania, Philadelphia, PA 19104, USA;*
[3]*Department of Physics and James Franck and Enrico Fermi Institutes, The University of Chicago, Chicago, Illinois 60637, USA*
(Dated: October 19, 2017)

We consider the contribution to the density of vibrational states and the distribution of energy barrier heights of incipient instabilities in a glass modeled by a jammed packing of spheres. On approaching an instability, the frequency of a normal mode and the height of the energy barrier to cross into a new ground state both vanish. These instabilities produce a contribution to the density of vibrational states that scales as ω^3 at low frequencies ω, and a contribution to the distribution of energy barriers ΔH that scales as $\Delta H^{-1/3}$ at low barrier heights.

Disordered solids inhabit an extremely high-dimensional rugged energy landscape with a vast number of metastable minima [1, 2]. Dealing with such a complex topography poses challenges for understanding how the system moves among metastable basins as a result of thermal excitations or external perturbations such as compression or shear. Here we focus on instabilities induced in zero-temperature ($T = 0$) systems by applied compression or shear as a first step in understanding how a disordered solid traverses its landscape.

When a system in a given energy basin becomes unstable at $T = 0$, a potential-energy barrier must vanish along some direction in configurational space so that the curvature vanishes in this direction implying a mode of vibration with frequency $\omega = 0$ [3–7]. As a result, low-frequency quasilocalized modes have particularly low energy barriers [8–11] and contain predictive information about incipient instabilities [12] that are spatially localized, and can be identified via anharmonic analysis of the energy landscape [13–16] as well as by purely structural measures [17].

Zero-temperature jammed sphere packings provide special insight into this physics. At the jamming transition, the density of states, $D(\omega)$, is nearly constant down to arbitrarily low ω [18, 19] and the removal of a single bond leads to the creation of a zero-frequency mode. At densities above the transition (i.e., at non-zero pressure), the packings are susceptible to small (but finite) perturbations that push the system into new energy minima [10, 20–24]. At low temperatures, one expects the lowest energy barriers to control how the system explores its landscape; the study of instabilities at $T = 0$ thus provides insight into behavior beyond the harmonic approximation.

In this paper, we study jammed packings in three dimensions and calculate $D(\omega)$ and the distribution, $P_H(\Delta H)$, of energy barriers ΔH corresponding to the most vulnerable directions in the energy landscape for encountering an instability. These distribution functions depend on the distance to the jamming transition. The contribution of incipient instabilities to $D(\omega)$ scales as ω^3 for both compression and shear. The number of *compression* instabilities per strain scales with system size, N, in such a way that their contribution to $D(\omega)$ vanishes in the thermodynamic limit. However, the number of *shear* instabilities per strain has a stronger dependence on N, consistent with earlier results [25]. This leads to a contribution to $D(\omega)$ that survives in the thermodynamic limit. We also find that the distribution of energy barriers corresponding to incipient instabilities varies as $P_H(\Delta H) \propto \Delta H^{-1/3}$ so that in the thermodynamic limit the system is marginally stable. By marginal stability, we mean that an infinitesimal perturbation can push the system over an energy barrier into a new ground state. Our results lead to a refined understanding of marginal stability in jammed packings.

Fold instability: We first review the expected scaling of the lowest vibrational mode frequency and barrier height as the system is compressed or sheared towards the stress τ_i at which the instability occurs. For compression, τ is the pressure p; for shear, τ is the shear stress Σ. We control τ, so the relevant landscape is the enthalpy landscape. The enthalpy of a system is $H = U + pV$ for compression, and its counterpart is $H = U - \Sigma\gamma V$ for shear [26], where U, V, and γ are the potential energy, volume, and shear strain, respectively. Consider $H(x)$ along the "reaction coordinate" x in configurational space. Assume that the saddle point is at $x = 0$ when $\tau = \tau_i$, as shown in Fig. 1(a). There is no linear or quadratic term in x since the system is unstable at τ_i and the curvature (or the square of the mode frequency) must vanish. H must therefore generically be cubic in x. We now retreat from the instability, so that $\tau < \tau_i$. The lowest non-vanishing coupling between $\delta\tau \equiv \tau_i - \tau$ and x is generically linear:

$$H = -\frac{1}{3}a_3x^3 + cx\delta\tau. \tag{1}$$

Here we assume that $a_3 > 0$, so that at $\delta\tau = 0$ (at the instability) the system is unstable towards a minimum

that lies at $x > 0$. The linear term shifts the minimum to $x_0 = -\sqrt{c\delta\tau/a_3}$ ($c > 0$), as shown in Fig. 1(a). Expanding H around $x = x_0$ in Eq. (1), we find

$$H = \frac{2}{3}a_3x_0^3 - a_3x_0(x-x_0)^2 - \frac{1}{3}a_3(x-x_0)^3 + \mathcal{O}[(x-x_0)^4]. \quad (2)$$

Therefore $\omega_L^2 = -2a_3x_0 = 2\sqrt{ca_3\delta\tau}$, where ω_L, the frequency of the mode associated with the instability, is

$$\omega_L = (4ca_3)^{1/4}(\delta\tau)^{1/4}. \quad (3)$$

This typical scaling of a fold instability [27] has long been observed in studies of soft modes in glassy systems [3–6]. The energy-barrier height scales as

$$\Delta H = \frac{4}{3}\frac{c^{3/2}}{a_3^{1/2}}(\delta\tau)^{3/2}. \quad (4)$$

Simulations: We confirm this scaling using numerical simulations of three-dimensional systems of $N \in [250, 4000]$ frictionless spheres. We consider jammed packings with a Hertzian interaction potential [28] between particles i and j:

$$U(r_{ij}) = \frac{2\epsilon}{5}\left(1 - \frac{r_{ij}}{\sigma_{ij}}\right)^{5/2}\Theta\left(1 - \frac{r_{ij}}{\sigma_{ij}}\right), \quad (5)$$

where r_{ij} and σ_{ij} are the separation between particles i and j and sum of their radii respectively, ϵ is the characteristic energy, and $\Theta(x)$ is the Heaviside step function. Periodic boundary conditions are applied in all directions in the absence of shear; in the case of shear, we use Lees-Edwards boundary conditions [29]. We study a 50:50 mixture of particles with diameters σ and $\sigma_L = 1.4\sigma$, respectively. All particles have the same ϵ and mass m. The units of length, mass, and energy are σ, m, and ϵ. The frequency has units $\sqrt{\epsilon/m\sigma^2}$.

By rapidly quenching ideal-gas states to $T = 0$ using a fast inertial relaxation engine algorithm [30], we minimize the enthalpy at fixed pressure to obtain mechanically stable disordered solids. For each system size, we generate 5000 distinct states at the desired pressure p. To study compression instabilities, we then compress each state by increasing p while minimizing the enthalpy, until there is an abrupt change of volume or packing fraction corresponding to the first instability for that initial state. To study shear instabilities, we apply shear stress Σ in the analogous quasistatic fashion and minimize the enthalpy, until there is an abrupt change of the shear strain γ. To calculate the vibration modes, we diagonalize the Hessian matrix corresponding to the appropriate generalized free energy using ARPACK [31].

Figures 1(b)-(d) show examples of the approach to a compression and a shear instability at p_i and Σ_i, respectively [32]. The packing fraction ϕ or shear strain γ is shown versus p or Σ in Fig. 1(b). At $p = p_i$ or $\Sigma = \Sigma_i$ ($\delta\tau = 0$), the bulk or shear modulus vanishes [33, 34].

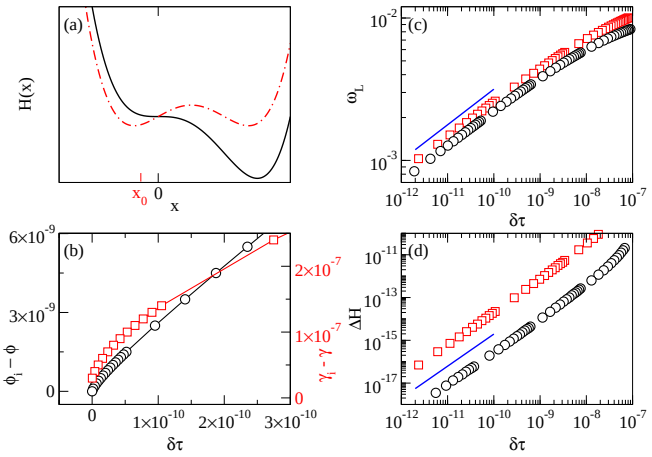

FIG. 1: (a) Schematic plot of the enthalpy landscape H along the reaction coordinate x at the stress corresponding to the instability, τ_i (solid), and at a stress below the instability, $\tau < \tau_i$ (dot-dashed), where the minimum is shifted to x_0. (b) Examples of the response of packing fraction ϕ and shear strain γ to the increase of stress τ upon approaching the compression (circles) and shear (squares) instabilities at ϕ_i and γ_i, where $\delta\tau \equiv \tau_i - \tau$. The lines are guides for the eye. (c)-(d) Frequency ω_L and enthalpy barrier height ΔH for the mode associated with the instability as a function of $\delta\tau$ for compression (circles) and shear (squares). The lines in (c) and (d) indicate the expected power law scalings $\omega_L \sim \delta\tau^{1/4}$ and $\Delta H \sim \delta\tau^{3/2}$, respectively.

The frequency of the mode associated with the instability, ω_L, is shown in Fig. 1(c) as we approach the instability. As expected, $\omega_L \sim \delta\tau^{1/4}$ for both compression and shear. In addition, Fig. 1(d) shows that the height of the enthalpy barrier vanishes on approaching the instability as $\Delta H \sim \delta\tau^{3/2}$, as expected.

Distribution functions: The values of the distance to the nearest instability, $\delta\tau$ and the variables c and a_3 defined in Eq. (1), vary from one enthalpy minimum to another, and can also depend on whether the instabilities are due to compression or shear. For an ensemble of initial enthalpy minima, we characterize the ensembles of compression and shear instabilities in terms of their respective distributions: $P_\tau(\delta\tau)$ for the distance to the nearest instability; $P_{\tau c}(c)$ for the coupling constant c; and $P_{\tau a}(a_3)$ for the cubic coefficient a_3.

Figure 2(a) shows that $P_\tau(\delta\tau)$ is approximately constant with increasing $\delta\tau$ until it falls off at $\delta\tau_y$ for both compression and shear. Because we calculate only the distance from τ to the *first* instability (at τ_i), $\delta\tau_y$ corresponds to the yield stress and is comparable to the stress interval between instabilities. The distributions for different system sizes collapse when $\delta\tau$ is scaled by N^{α_N} with $\alpha_N = 0.33 \pm 0.05$ for compression and 0.65 ± 0.06 for shear. This implies that $\delta\tau_y \propto N^{-\alpha_N}$. The same scaling of the distance between shear instabilities has been observed in several models with decaying power-law inter-

actions, including Lennard-Jones systems [5, 25, 35, 36]. It is associated with an exponent $\theta_e > 0$ characterizing the distribution of yield stresses as well as the existence of avalanches [37, 38], such that $\delta\Sigma_y \propto N^{-1/(\theta_e+1)}$. Sublinear scalings in $1/N$ are also seen in calculations of energy barriers in mean-field spin glasses [39, 40], where this decrease may be associated with the fractal nature of the energy landscape – a feature also predicted for jammed packings in infinite dimensions [41].

Figure 2(b) shows how $P_\tau(\delta\tau)$ depends on the initial pressure p: $\delta\tau_y \propto p^{\alpha_p}$ with $\alpha_p = 0.73 \pm 0.03$ for compression and 1.08 ± 0.05 for shear. As expected, the yield stress vanishes as the jamming transition is approached.

Figure 2(c) shows that the distribution of c is independent of N and is fairly innocuous with a peak at $c \approx 0.16$ for compression and $c \approx 1.6$ for shear, when $p = 10^{-3}$. Figure 2(d) shows that the shape of the c distribution does not change appreciably with pressure. We find that the peak position c_{max} and amplitude $P_{\tau c,max}$ are $(0.10, 5.15)$, $(0.16, 3.92)$ and $(0.20, 3.49)$ for compression and $(1.78, 0.31)$, $(1.55, 0.34)$, and $(1.54, 0.38)$ for shear, at pressures $p = 10^{-4}, 10^{-3}$ and 10^{-2}, respectively.

The distributions of cubic coefficient, $P_{\tau a}(a_3)$, are within numerical error for compression and shear, as shown in Figs. 2(e) and 2(f). For both cases, there is a broad, approximately power-law, distribution of a_3 that is cut off at low values of a_3. As N increases, the minimum shifts to lower a_3 as $N^{-0.3\pm0.1}$ for both compression and shear. As the pressure is reduced towards the jamming transition, the distribution appears to approach a pure power law of $P(a_3) \sim a_3^{-1.0}$ at small a_3, as the peak value vanishes approximately as $p^{0.75\pm0.05}$.

Density of states and energy barriers: We now consider the contribution of compression and shear instabilities to the density of states, $D(\omega)$, and the distribution of energy barriers, $P_H(\Delta H)$, at a given pressure p and at $\Sigma = 0$. An incipient instability at τ_i will contribute a mode at a frequency given by Eq. (3) and a barrier height given by Eq. (4). The contribution of instabilities to $D(\omega)$ or to $P_H(\Delta H)$ is therefore the sum over the contributions of all of the incipient instabilities. The number of compression instabilities in a given pressure interval is $\mathcal{P}_p \propto 1/\delta p_y \sim N^{0.33} p^{-0.73}$. Similarly, the number of shear instabilities in a given shear-stress interval is $\mathcal{P}_\Sigma \propto 1/\delta\Sigma_y \sim N^{0.65} p^{-1.08}$. The contribution of either compression or shear instabilities to the normalized density of states is

$$D(\omega) = \frac{\mathcal{P}_\tau}{3N} \int_\tau^\infty d\tau_i \int_0^\infty da_3 P_{\tau a}(a_3) \int_0^\infty dc P_{\tau c}(c) \delta(\omega - \sqrt{2}(c a_3 \delta\tau)^{1/4}), \quad (6)$$

where the lower limit of the first integral is $\tau = p$ for compression instabilities and $\tau = 0$ for shear instabilities.

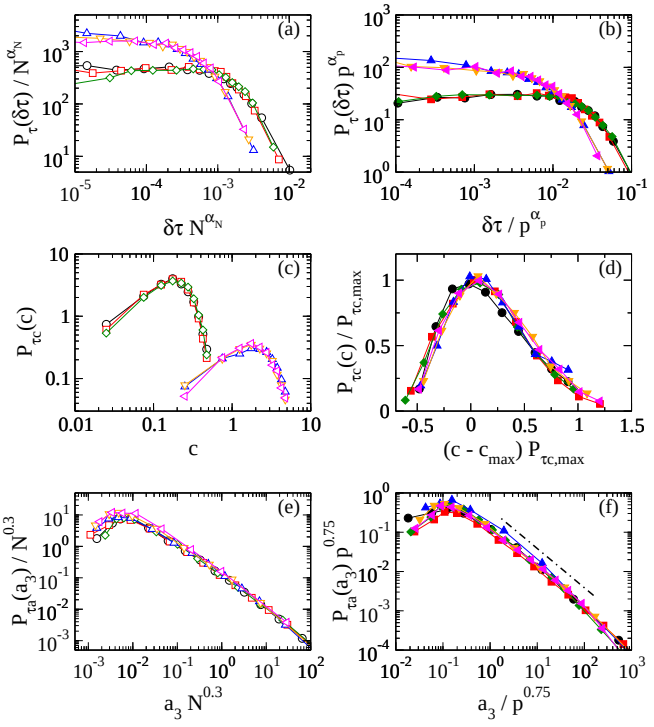

FIG. 2: (Left column) System-size and (Right column) pressure dependence of the distributions of $\delta\tau$, c and a_3 characterizing compression and shear instabilities. For the left column, system sizes are $N = 250$, 1000, and 4000 (circles, squares, and diamonds for compression; upward, downward, and leftward triangles for shear), all at $p = 10^{-3}$. For the right column, pressures are $p = 10^{-4}$, 10^{-3}, and 10^{-2} (circles, squares, and diamonds for compression; upward, downward, and leftward triangles for shear), all at $N = 1000$. Lines are guides for the eye. The dot-dashed line in (f) has a slope of -1.

The contribution to the distribution of energy barriers is

$$P_H(\Delta H) = \mathcal{P}_\tau \int_\tau^\infty d\tau_i \int_0^\infty da_3 P_{\tau a}(a_3) \int_0^\infty dc P_{\tau c}(c) \delta(\Delta H - \frac{4}{3} c^{3/2} a_3^{-1/2} (\delta\tau)^{3/2}). \quad (7)$$

In the low-frequency limit, Eq. (6) leads to

$$D(\omega) = \frac{\mathcal{P}_\tau \langle a_3^{-1} \rangle_\tau \langle c^{-1} \rangle_\tau}{3N} \omega^3, \quad (8)$$

where $\langle a_3^{-1} \rangle_\tau = \int_0^\infty da_3 P_{\tau a}(a_3) a_3^{-1}$ and $\langle c^{-1} \rangle_\tau = \int_0^\infty dc P_{\tau c}(c) c^{-1}$.

Equation (8) shows that both compression and shear instabilities give rise to an ω^3 contribution to $D(\omega)$. The scalings in Fig. 2 show that the contribution to $D(\omega)$ vanishes as $N^{-0.37\pm0.15}$as $N \to \infty$ for compression instabilities, so that they do not contribute to the density of normal modes of vibration in the thermodynamic limit. For shear instabilities, there is a different scaling of $\mathcal{P}_\Sigma$ than there is for $\mathcal{P}_p$: $\mathcal{P}_\Sigma \sim N^{0.65\pm0.06}$. (However, the

scaling of $\langle a_3^{-1}\rangle_\Sigma$ is the same within our numerical uncertainty as that for $\langle a_3^{-1}\rangle_p$). From Eq. (8) we see that for shear instabilities, the N-dependence of the contribution to $D(\omega)$ scales as $N^{-0.05\pm0.16}$, so that there is no N-dependence within measurement error. This implies that the contribution of shear instabilities to the density of states survives in the thermodynamic limit.

For low energy barriers, we find from Eq. (7)

$$P_H(\Delta H) = (\frac{1}{6})^{1/3}\mathcal{P}_\tau\langle a_3^{1/3}\rangle_\tau\langle c^{-1}\rangle_\tau\Delta H^{-1/3}, \quad (9)$$

for both compression and shear instabilities. Note that if $P_{\tau a}(a_3) \sim 1/a_3$ at large a_3, as suggested by the dot-dashed line in Fig. 2(f), then $\langle a_3^{1/3}\rangle_\tau$ diverges at the high a_3 (low energy barrier) end. A closer look at Fig. 2(f), however, suggests that $P_{\tau a}(a_3)$ bends down more rapidly than $1/a_3$ at high a_3. We therefore assume that $\langle a_3^{1/3}\rangle_\tau$ is finite. In that case, P_H increases with $\mathcal{P}_p\langle a_3^{1/3}\rangle_p \propto p^{-0.48\pm0.05}$ for compression instabilities and $\mathcal{P}_\Sigma\langle a_3^{1/3}\rangle_\Sigma \propto p^{-0.83\pm0.07}$ for shear instabilities.

Discussion and conclusions: Sphere packings with soft, finite-ranged repulsions are marginally stable to extended instabilities at the jamming transition at zero pressure, where there are the minimum number of contacts needed for mechanical stability [18, 20]. As the system is compressed above the transition, the connectivity increases, but at a pressure p, the system is still close to the limit of stability with respect to compression – it is just slightly above the minimum connectivity needed to support that pressure against extended instabilities [10, 24]. One main conclusion of our analysis is that a finite-sized jammed solid is nearly marginally stable with respect to compression or shear and becomes marginally stable in the thermodynamic limit. In that limit an infinitesimal increase in either stress will lead to an instability and the vanishing of a mode frequency. These instabilities are only a subset of all possible localized instabilities that can be triggered by applied stresses. Simulations have demonstrated that low-frequency, localized, anharmonic modes in jammed systems can produce echo phenomena [42]. The low-frequency modes arising from these instabilities might provide a source for the phonon echoes observed in experiments but which have previously been ascribed to quantum-mechanical two-level systems [43].

A consequence of marginal stability to localized instabilities is the predicted contribution of ω^3 to the density of states. A low-frequency density of states scaling as ω^2 (consistent with mean-field expectations [44]) has been reported [45] while others find ω^4 [46, 47]. The ω^4 scaling has been predicted for stable finite-size disordered systems [48] and typically dominates for finite systems, which are stable to localized instabilities. However, it has recently been reported that the low-frequency density of states for a $T = 0$ disordered glass of particles with inverse power-law repulsions scales as $D(\omega) \sim \omega^3$ if the glasses were prepared by sufficiently rapid quenching from a sufficiently high temperature [49]. For sufficiently slow quenches from lower temperatures, $D(\omega) \sim \omega^4$ was found for $N = 2000$ particle systems. These findings are consistent with our results. Rapidly-quenched systems should have more "soft spots" [12] or equivalently, more incipient instabilities than slowly-quenched systems. Thus, the number of instabilities per stress interval, $\mathcal{P}_\tau$, should be higher for rapidly-quenched systems, possibly leading to a dominant ω^3 contribution even in finite systems.

One interesting conclusion from our results is that the nature of the ground states in jammed systems has universal anharmonic as well as harmonic properties. Harmonic properties such as the elastic moduli and density of vibrational states are universal in jammed packings of particles with repulsive, finite-ranged potentials and the existence of universal anharmonic features has previously been hinted at in jammed systems [8]. The anharmonic features studied here, however, are likely to be even more broadly universal because they originate from the scaling of the fold instability. Such instabilities have been found in Lennard-Jones glasses [3–6] and the scaling of the shear yield stress for our jammed packings is the same as that observed earlier for Lennard-Jones glasses [25]. As long as the distribution of a_3 has finite and nonzero values of $\langle a_3^{-1}\rangle$ and $\langle a_3^{1/3}\rangle$, the scalings we predict for the density of states and energy barrier distribution should hold.

We thank H. H. Boltz, E. Corwin, M. L. Manning, G. Parisi, S. Ridout, S. S. Schoenholz, J. P. Sethna, D. M. Sussman, and F. Zamponi for instructive discussions. This work was supported by the National Natural Science Foundation of China Grants No. 21325418 and No. 11574278 (NX), Fundamental Research Funds for the Central Universities Grant No. 2030020028 (NX), and by the Simons Foundation for the collaboration "Cracking the Glass Problem" (454945 to AJL and 348125 to SRN) and the U.S. Department of Energy, Office of Basic Energy Sciences, Division of Materials Sciences and Engineering under Grants No. DE-FG02-05ER46199 (AJL, NX) and No. DE-FG02-03ER46088 (SRN,NX).

[1] F. H. Stillinger and T. A. Weber, Phys. Rev. B **31**, 5262 (1985).
[2] P. G. Debenedetti and F. H. Stillinger, Nature **410**, 259 (2001).
[3] D. L. Malandro and D. J. Lacks, Phys. Rev. Lett. **81**, 5576 (1998).
[4] D. L. Malandro and D. J. Lacks, J. Chem. Phys. **110**, 4593 (1999).
[5] C. E. Maloney and A. Lemaitre, Phys. Rev. Lett. **93**, 016001 (2004).
[6] C. E. Maloney and A. Lemaitre, Phys. Rev. E **74**, 016118 (2006).
[7] Note that these instabilities are distinct from events that

change the contact network but do not lead to the vanishing of a low-frequency mode [12].
[8] N. Xu, V. Vitelli, A. J. Liu, and S. R. Nagel, Europhys. Lett. **90**, 56001 (2010).
[9] N. Xu, M. Wyart, A. J. Liu, and S. R. Nagel, Phys. Rev. Lett. **98**, 175502 (2007).
[10] E. deGiuli, A. Laversanne-Finot, G. Duering, E. Lerner, and M. Wyart, Soft Matter **10**, 5628 (2014).
[11] V. Vitelli, N. Xu, M. Wyart, A. J. Liu, and S. R. Nagel, Phys. Rev. E **81**, 021301 (2010).
[12] M. L. Manning and A. J. Liu, Phys. Rev. Lett. **107**, 108302 (2011).
[13] L. Gartner and E. Lerner, Phys. Rev. E **93**, 011001(R) (2016).
[14] L. Gartner and E. Lerner, SciPost Phys. **1**, 016 (2016).
[15] E. Lerner, Phys. Rev. E **93**, 053004 (2016).
[16] J. Zylberg, E. Lerner, Y. Bar-Sinai, and E. Bouchbinder, arXiv:1703.09014.
[17] E. D. Cubuk, S. S. Schoenholz, J. M. Rieser, B. D. Malone, J. Rottler, D. J. Durian, E. Kaxiras, and A. J. Liu, Phys. Rev. Lett. **114**, 108001 (2015).
[18] C. S. O'Hern, L. E. Silbert, A. J. Liu, S. R. Nagel, Phys. Rev. E **68**, 011306 (2003).
[19] L. E. Silbert, A. J. Liu and S. R. Nagel, Phys. Rev. Lett. **95**, 098301 (2005).
[20] A. J. Liu and S. R Nagel, Ann. Rev. Cond. Mat. Phys. bf 1, 347 (2010).
[21] M. van Hecke M, J. Phys. Condens. Matter **22**, 033101 (2010).
[22] A. J. Liu, M. Wyart, and S. R. Nagel, *The jamming scenario-an introduction and outlook* in *Dynamical heterogeneities in glasses, colloids and granular materials*, Eds.: L. Berthier, G. Biroli, J.-P. Bouchaud, L. Cipelletti, and W. van Saarloos (2011).
[23] M. Wyart, Ann. de Physique **30**, 1 (2005).
[24] M. Müller and M. Wyart, Annu. Rev. Cond. Mat. Phys. **6**, 177 (2015).
[25] K. M. Salerno and M. O. Robbins, Phys. Rev. E **88**, 062206 (2013).
[26] H. Liu, X. Xie, and N. Xu, Phys. Rev. Lett. **112**, 145502 (2014).
[27] V. Arnold, *Catastrophe Theory*, 3rd Ed. (Springer-Verlag, Berlin, 1992).
[28] We use the Hertzian instead of the harmonic potential so that there is no discontinuity in the second derivative of the potential at the point of contact.
[29] M. P. Allen and D. J. Tildesley, *Computer simulation of liquids* (Oxford University Press, New York, 1987).
[30] E. Bitzek, P. Koskinen, F. Gahler, M. Moseler, and P. Gumbsch, Phys. Rev. Lett. **97**, 170201 (2006).
[31] http://www.caam.rice.edu/software/ARPACK.
[32] See Supplemental Material at http://link.aps.org/supplemental for additional information about the particle movement on approaching instabilities.
[33] In earlier studies of sheared glasses [5, 6], in which instabilities were induced by applying shear, the shear modulus actually became negative before the instability. This unphysical result arises because the system was held at fixed volume and box shape [34].
[34] S. Dagois-Bohy, B. P. Tighe, J. Simon, S. Henkes, and M. van Hecke, Phys. Rev. Lett. **109**, 095703 (2012).
[35] S. Karmakar, E. Lerner, and I. Procaccia, Phys. Rev. E **82**, 055103 (2010).
[36] K. M. Salerno, C. E. Maloney, and M. O. Robbins, Phys. Rev. Lett. **109**, 105703 (2012).
[37] J. Lin, E. Lerner, A. Rosso, and M. Wyart, Proc. Natl. Acad. Sci. USA **111**, 14382 (2014).
[38] J. Lin, A. Saade, E. Lerner, A. Rosso, and M. Wyart, Europhys. Lett. **105**, 26003 (2014).
[39] A. Cavagna, I. Giardina, and G. Parisi, Phys. Rev. Lett. **92**, 120603 (2004).
[40] T. Aspelmeier, R. A. Blythe, A. J. Bray, and M. A. Moore, Phys. Rev. B **74**, 184411 (2006).
[41] P. Charbonneau, J. Kurchan, G. Parisi, P. Urbani, and F. Zamponi, Nat. Comm. **5**, 3725 (2014).
[42] J. C. Burton and S. R. Nagel, Phys. Rev. E **93**, 032905 (2016).
[43] B. Golding, J. E. Graebner, Phys. Rev. Lett. **37**, 852 (1976).
[44] A. Altieri, S. Franz, and G. Parisi, J. Stat. Mech., 093301 (2016).
[45] P. Charbonneau, E. I. Corwin, G. Parisi, A. Poncet, and F. Zamponi, Phys. Rev. Lett. **117**, 045503 (2016).
[46] E. Lerner, G. During, and E. Bouchbinder, Phys. Rev. Lett. **117**, 035501 (2016).
[47] H. Mizuno and A. Ikeda, arXiv:1703.10004.
[48] V. Gurarie and J. T. Chalker, Phys. Rev. B **68**, 134207 (2003).
[49] E. Lerner, arXiv:1705.01037.